ISSN 0021-3640, JETP Letters, 2016, Vol. 104, No. 6, pp. 392–397. © Pleiades Publishing, Inc., 2016.
Published in Russian in Pis'ma v Zhurnal Eksperimental'noi i Teoreticheskoi Fiziki, 2016, Vol. 104, No. 6, pp. 406–412.

CONDENSED MATTER

Phonon Assisted Resonant Tunneling and Its Phonons Control[1]

F. V. Kusmartsev[a, *], V. D. Krevchik[b], M. B. Semenov[b, **], D. O. Filatov[c], A. V. Shorokhov[d], A. A. Bukharaev[e, f], Y. Dakhnovsky[g], A. V. Nikolaev[h, i], N. A. Pyataev[d], R. V. Zaytsev[b], P. V. Krevchik[b], I. A. Egorov[b], K. Yamamoto[j], and A. K. Aringazin[k]

[a] *Department of Physics, Loughborough University, LE11 3TU Loughborough, United Kingdom*
[b] *Department of Physics, Penza State University, Penza, 440026 Russia*
[c] *Lobachevsky State University of Nizhny Novgorod, Nizhny Novgorod, 603950 Russia*
[d] *Mordovia State University, Saransk, 430005 Russia*
[e] *Zavoisky Institute for Physics and Technology, Kazan Scientific Center, Russian Academy of Science, Kazan, 420029 Russia*
[f] *Kazan Federal University, Kazan, 420008 Russia*
[g] *Department of Physics and Astronomy, University of Wyoming, WY 82071 Laramie, USA*
[h] *Skobeltsyn Institute of Nuclear Physics, Moscow State University, Moscow, 119991 Russia*
[i] *Moscow Institute of Physics and Technology (State University), Dolgoprudnyi, Moscow region, 141700 Russia*
[j] *Research Institute, International Medical Center, 2-25-22-304 Kohinata Bunkyo-ku, Tokyo, Japan*
[k] *Institute for Basic Research, Eurasian National University, Astana, 010008 Kazakhstan*
** e-mail: F.Kusmartsev@lboro.ac.uk*
*** e-mail: misha29.02@gmail.com*

Received February 12, 2016; in final form, August 1, 2016

We observe a series of sharp resonant features in the tunneling differential conductance of InAs quantum dots. We found that dissipative quantum tunneling has a strong influence on the operation of nanodevices. Because of such tunneling the current–voltage characteristics of tunnel contact created between atomic force microscope tip and a surface of InAs/GaAs quantum dots display many interesting peaks. We found that the number, position, and heights of these peaks are associated with the phonon modes involved. To describe the found effect we use a quasi-classical approximation. There the tunneling current is related to a creation of a dilute instanton–anti-instanton gas. Our experimental data are well described with exactly solvable model where one charged particle is weakly interacting with two promoting phonon modes associated with external medium. We conclude that the characteristics of the tunnel nanoelectronic devices can thus be controlled by a proper choice of phonons existing in materials, which are involved.

DOI: 10.1134/S0021364016180016

1. INTRODUCTION

One of the practical problems in semiconductor tunnel nanoelectronics is to extend control over parameters of quantum tunnel effect of electrons [1–12]. Physical and chemical approaches to electron transfer processes at nanoscales reveal some common tools. Namely, analytical models of multidimensional dissipative simultaneous quantum tunneling of one or two charged particles, electrons or protons, in low-dimensional systems used in studying some chemical reactions at low temperatures [6–17], can be used to study physical properties of quantum dots (QDs) [7, 18–20].

Quasiclassical, dilute instanton–anti-instanton gas approach to the dissipative quantum tunneling of particles interacting with heat bath is known to be powerful technique in obtaining analytical results, starting from a classical action of the system [1–4]. In particular, probability rate of quantum tunneling of two mutually interacting charged particles moving in medium, which occurs in synchronous or asynchronous modes, was studied in our previous work [16].

The purpose of the present work is to identify experimentally observed dissipative tunneling effects predicted by the theory developed in the pioneering works of A.J. Leggett, A.I. Larkin, Yu.N. Ovchinnikov, et al. In this paper, we show results of our recent experimental study of the effect of wide-band matrix on semiconductor InAs/GaAs(001) QDs which

[1] The article is published in the original. Supplementary material is available at http://link.springer.com/.

changes some macroscopic properties of the system, and can be identified by the tunnel current–voltage (I–V) relation of the tunnel device. Parameter associated to this effect can be treated as one more controllable parameter of nanostructures, in addition to energy levels of QD, which are controlled by its size parameter. Note that the role of wide-band matrix in taking control over mesoscopic systems has been stressed in [5]. In addition, we develop and apply 1D dissipative tunneling model accounting for influence of *two* promoting phonon modes coming from the wide-band matrix, to study quantum tunneling in the structure of single QDs by Conducting Atomic Force Microscopy (CAFM). We make a comparison of the obtained theoretical tunneling probability rate in an oscillatory regime with the experimental I–V relation of the contact between Atomic Force Microscopy (AFM) probe and InAs/GaAs(001) QD surface.

2. 1D DISSIPATIVE TUNNELING PROBABILITY RATE WITH ACCOUNT FOR TWO LOCAL PHONON MODES IN THE WIDE-BAND MATRIX

We start with short description of the dissipative tunneling approach, which will be used in formulating our specific model. Let p_1 be the momentum of the tunneling particle, y_1 be the coordinate of the tunneling particle, and v_1 be the two-well potential. Then, the Hamiltonian

$$\hat{H} = \frac{p_1^2}{2} + v_1(y_1) + y_1\sum_{\alpha=2}^{N} C_\alpha y_\alpha + \frac{1}{2}\sum_{\alpha=2}^{N}\left(p_\alpha^2 + \omega_\alpha^2 y_\alpha^2\right) \quad (1)$$

describes particle in the model asymmetric two-well oscillatory potential v_1 along the tunnel coordinate y_1. In Eq. (1) p_α are momenta of phonon modes of the particle of mass $m = 1$, y_α are coordinates of local phonon modes, ω_α are frequencies of local phonon modes, N is the number of local modes of wide-band matrix, and C_α are coefficients of the interaction of the tunneling particle with local phonon modes of wide-band matrix (see [13, 16, 17] for more details).

The quasiclassical action $S\{y_1\}$ of the system is defined by [16]

$$S\{y_1\} = \int_{-\beta/2}^{\beta/2} d\tau\left[\frac{1}{2}\dot{y}_1^2 + v(y_1) + \frac{1}{2}\int_{-\beta/2}^{\beta/2} d\tau' K(\tau-\tau')\, y_1(\tau) y_1(\tau')\right]. \quad (2)$$

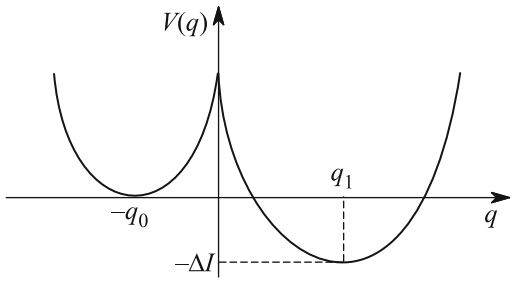

Fig. 1. Asymmetric two-well oscillatory potential along the tunnel coordinate q of the model.

Hereafter, the overdot denotes the derivative with respect to τ, $\beta = 2\pi h/k_B T$ is the inverse temperature, $K(\tau) = T\sum_{\omega_n} K(\omega_n)\exp(-i\omega_n\tau)$ is the Matsubara Green's functions [1, 2], where $K(\omega_n) = -\sum_\alpha C_\alpha^2/(\omega_\alpha^2 + \omega_n^2)$ and $\omega_n = 2\pi Tn$, and the renormalized potential $v(y_1)$ is given by the expression

$$v(y_1) = v_1(y_1) - \frac{1}{2}\sum_{\alpha=2}^{N}\frac{C_\alpha^2}{\omega_\alpha^2} y_1^2. \quad (3)$$

The form of the potential v as a function of the renormalized coordinate q is shown in Fig. 1. The procedures of the renormalization of the potential $v_1(y_1)$ and the coordinate y_1 are considered in [17].

In the instanton approximation, 1D Euclidean action S_B for one charged particle in the two-well renormalized oscillator potential and the external electric field E is found as [13, 14, 18]

$$S_B = 2\omega_0^2(q_0+q_1)q_0\tau_0 - \frac{2\omega_0^2(q_0+q_1)^2\tau_0^2}{\beta} - \frac{4\omega_0^4(q_0+q_1)^2}{\beta}\sum_{n=1}^{\infty}\frac{\sin^2\nu_n\tau_0}{\nu_n^2\left(\nu_n^2+\omega_0^2+\zeta_n\right)}, \quad (4)$$

where e is charge of the particle, $q_0 = b^* - |e|E/\omega_0^2$ and $q_1 = b^* + |e|E/\omega_0^2$ are parameters of the renormalized two-well potential in the external electric field E, $\pm b^*$ are positions of the minima of the potential in zero-field case, τ_0 is the instanton center, ω_0 is the oscillator potential frequency, $\nu_n = 2\pi n/\beta$ is Matsubara frequency, $n = 1, 2, 3, \ldots$, and ζ_n is the Fourier component of the viscous core of the corresponding quasiclassical Euler–Lagrange equation of motion,

$$\zeta_n = \nu_n^2\sum_{\alpha=2}^{N}\frac{C_\alpha^2}{\omega_\alpha^2\left(\omega_\alpha^2+\nu_n^2\right)}. \quad (5)$$

The probability of quantum tunneling of the particle through the barrier shown in Fig. 1 per unit time

$\Gamma = B\exp(-S_B)$ contains pre-exponential factor B, the most contribution to which is made by the particle trajectories that are very close to the instanton. Expanding the action up to quadratic term in $q - q_B$, where q_B is the extremal instanton trajectory, and integrating over the functional space, we get

$$B = \left[\frac{S_0}{2\pi}\frac{\det\left(\frac{\delta^2 S}{\delta q^2}\right)_{q=-q_0}}{\det'\left(\frac{\delta^2 S}{\delta q^2}\right)_{q=q_B(\tau)}}\right]^{1/2}, \quad (6)$$

where

$$S_0 = \int_{-\beta/2}^{\beta/2} \dot{q}_B^2(\tau)d\tau. \quad (7)$$

Here, det' denotes determinant with zero eigenvalues corresponding to zero modes of the instanton omitted, and we used the approximation of dilute instanton–anti-instanton gas; i.e., the probability rate is much lower than the inverse width of the instanton,

$$\Gamma \ll (\Delta\tau)^{-1}. \quad (8)$$

We assume that the major contribution to the action $S\{q\}$ is made by the instanton, i.e., by the trajectory $q_B(\tau)$, which minimizes the action (4) and obeys the following Euler–Lagrange equation:

$$-\ddot{q}_B(\tau) + \frac{\partial v(q_B)}{\partial q_B} + \int_{-\beta/2}^{\beta/2} d\tau' K(\tau - \tau')q_B(\tau') = 0. \quad (9)$$

Here, the trajectory $q_B(\tau)$ is found within the class of periodic functions $q_B(\tau) = q_B(\tau + \beta)$. The form of the solution of Eq. (9) obeying this condition is shown in Fig. 2.

With the action (4), we obtain B from Eq. (6) as follows:

$$B = \frac{2\omega_0^2(q_0 + q_1)^2}{(2\pi\beta)^{1/2}} \times \sum_{n=-\infty}^{\infty}\frac{\sin^2\nu_n\tau_0}{\lambda_{0n}}\left(\sum_{n=-\infty}^{\infty}\frac{\cos 2\nu_n\tau_0}{\lambda_{0n}}\right)^{-1/2}. \quad (10)$$

Now we specify our model by assuming that the particle interacts weakly with two local phonon modes, i.e., $\omega_{L1} = \omega_2$ and $\omega_{L2} = \omega_3$.

We also make natural assumption that the interactions are weak, i.e., $C_\alpha/\omega_0^2 \ll 1$ and $C_\alpha/\omega_L^2 \ll 1$. In this case, we get

$$\zeta_n = \nu_n^2\frac{C_2^2}{\omega_2^2(\omega_2^2 + \nu_n^2)} + \nu_n^2\frac{C_3^2}{\omega_3^2(\omega_3^2 + \nu_n^2)}. \quad (11)$$

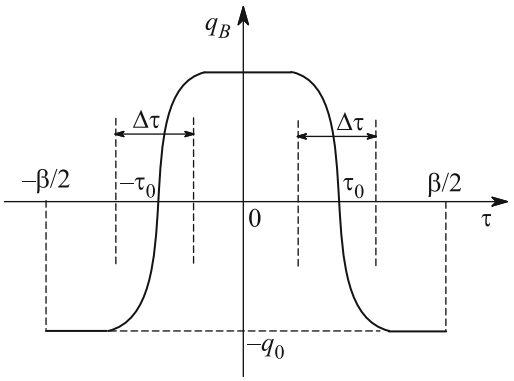

Fig. 2. Instanton $q_B(\tau)$, for $\tau > 0$, where τ_0 and $\Delta\tau$ are the so-called center and width of the instanton, respectively.

The tedious calculations provides analytical formulas for the optimal action $\tilde{S}_B$ and pre-exponential factor B. Due its large expression it is given in [21]. For a completeness, we should mention that there is a second solution that corresponds to the case of non-oscillating character of the probability rate. We shortly present the results for this case in [21].

3. EXPERIMENTAL SETUP

The experimental setup is shown in Fig. 3. Samples for the study were prepared on the n^+-GaAs(001) substrate doped by Sn using metalorganic chemical vapor deposition (MOCVD) at atmospheric pressure.

The n^+-GaAs buffer layer of 200 nm thickness doped by Si, with the donor concentration $N_D \simeq 10^{18}$ cm^{-3} has been grown at $T = 650°$C. The n-GaAs spacer layer with $N_D \simeq 10^{15}$ cm^{-3} of 3 nm thickness has been grown on the buffer layer. This layer forms triangular potential barrier between the QD and n^+-GaAs buffer layer [22]. The InAs QD has been formed by Stransky–Krastanov mechanism at $T = 530°$C. Nominal thickness of deposited InAs layer is about 1.5 nm.

The samples have been prepared at the Research Institute for Physics and Technology, Lobachevsky State University of Nizhny Novgorod, Russia, and then used to study spatial and energy distribution of the local density of states in InAs QD by the method of tunnel AFM, at the Zavoisky Institute for Physics and Technology, Kazan Scientific Center, Russian Academy of Science (Kazan, Russia).

Note that in [23] local density of states in InAs/GaAs(001) QDs was measured by CAFM. In [24] Scanning Tunneling Microscopy (STM) has been used in Ultra-High Vacuum (UHV) to measure local density of states in quantum wells GaSb/InAs. In [25] *combined* UHV STM/AFM has been implemented for the first time for the tunneling spectroscopy of the

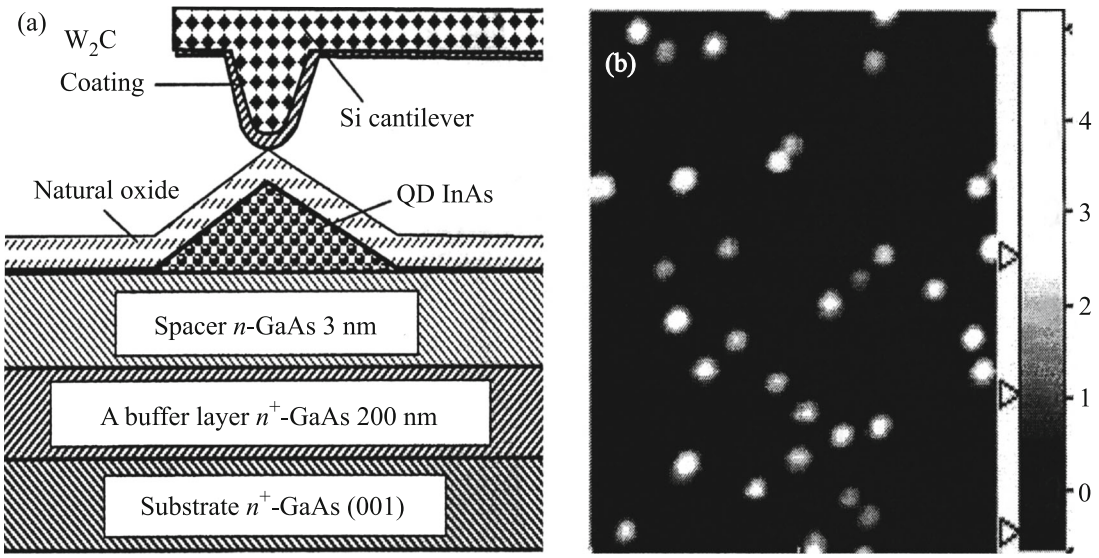

Fig. 3. (a) Schematic representation of the experimental setup for measuring the electric current between the AFM probe and the conductive substrate via the surface of InAs/GaAs(001) QD by CAFM. (b) AFM image of the surface of the 750 × 700-nm InAs/GaAs(001) QD structure in the range of heights of 5.9 nm.

size-quantized states in the InAs/GaAs (001) surface QDs. Tunneling spectra and current images, which reflect the energy and spatial distribution of the local density of the ground and excited states in the QDs have been obtained. Tunneling AFM technique and results of ex situ investigations of local density of states of quantum confined states in self-assembled semiconductor InAs/GaAs(001) QDs and InGaAs/GaAs InAs/GaAs(001) quantum rings, grown by Atmospheric Pressure Metal Organic Vapor Phase Epitaxy (AP-MOVPE), and GeSi/Si InAs/GaAs(001) nanoislands covered by native oxide have been presented in [26]. There samples with surface nanostructures were scanned across by conductive Si AFM probe covered by conductive coating (Pt, W_2C, or diamond-like film) in the contact mode. Main advantage of the tunneling AFM as compared to UHV STM is that the former allows ex situ investigation of the surface semiconductor nanostructures, which are naturally oxidized in ambient air when one takes samples from growth setup to AFM setup.

Our experiment was done at room temperatures under very high vacuum in a chamber with an Omicron UHV AFM/STM VT scanning probe microscope, which is a part of a very high vacuum Omicron MultiProbe P setup. Basic pressure in the chamber was about 10^{-10} Torr. Surface of the sample experienced oxidation in ambient air during the time of transportation from the growth setup to the vacuum chamber. It was scanned by p^+-Si probe with W_2C covering, in contact mode (see Fig. 3), with potential difference V_g between n^+-GaAs substrate and AFM probe.

In the experiment we have obtained spatial distributions of electric current I_t between AFM probe and the sample as a function of AFM probe coordinates (x, y) in the plane of sample's surface, at various constant V_g. We refer to these distributions as current images. They reflect spatial distribution of local density of states in the plane: wavefunction mappings [24] with a sum over energies below Fermi level of the probe. We do not present resulting current images here, and mention only that for the potential difference range $V_g = 2.6$–3.1 V across it, these reveal two maxima corresponding to p-symmetry of the excited states of QDs, while at lower voltages $V_g < 2.6$ V the current images have round form corresponding to the s-symmetry of the ground state [27].

The I–V relation of the contact between the AFM probe and QD have been obtained by measuring current images at different fixed V_g. More details on the used method of growth and tunnel spectroscopy of QD one can find, e.g., in [28].

Figure 3b represents AFM image of the surface of the studied sample. Surface QD has 5 to 6 nm thickness. It should be noted that lateral dimensions of QD shown in Fig. 3b are significantly larger than that expected for QD, 10 to 12 nm, which has form of tetrahedral pyramid with planes (101). This is explained by the effect of convolution related to the curvature of the AFM probe characterized by the radius $R_p \simeq 35$ nm.

4. COMPARISON WITH THE EXPERIMENT

We turn to a comparison of the obtained theoretical results for the 1D quantum tunneling probability rate

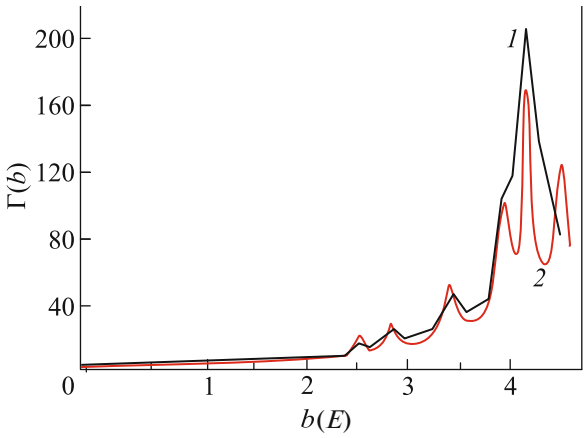

Fig. 4. (Color online) Comparison of the theoretical result (oscillatory case) for the 1D quantum tunneling probability rate Γ of the charged particle weakly interacting with the two local phonon modes of medium (curve *1*) as a function of the symmetry parameter b linearly depending on the external electric field intensity E with the experimental I–V relation for the probe-to-sample contact for InAs/GaAs(001) QD at 300 K (represented as curve *2*) obtained in the conductive atomic force microscopy experiment. Shown numerical values on the axes are in the units of applied voltage varied in the range $V_g = 0.0$–4.0 V with a step of 100 mV and an accuracy if 1 mV, and the current I in picoamperes measured with an accuracy of 10 pA.

of the charged particle weakly interacting with the two local phonon modes of medium with the experimental I–V relation of InAs/GaAs(001) QD measured by using CAFM.

In Fig. 4, we plot the experimental I–V relation and the obtained result for tunneling probability rate Γ, which we treat as proportional to the current I, as a function of the parameter $b = q_0$ linearly depending on the external electric field intensity E, which in turn linearly depends on the potential difference V across it.

Fitting parameters are the frequencies of local phonon modes and the coupling constants of the particle to these modes. Values of other parameters of the model, namely, the two-well potential parameters, temperature, and external electric field intensity were set due to the experiment.

The observed peaks are not due to Coulomb blockage because these are not equidistant. Sometimes these peaks are interpreted as the result of a resonance phenomenon in tunneling.

While the position of the highest theoretical peak meets the experimental one, its height underestimates the latter by about 20%. In addition, we note that the highest experimental peak reveals signs of two additional peaks matching two theoretical ones close to the highest peak. This can be explained by an approximate character of the used asymmetric two-well oscillatory potential.

The case of non-oscillating character of the probability rate obviously does not correspond to the experimental data. Nevertheless, we present shortly the results in the supplementary material [21]. This damping solution is valuable as it tells us that whether the rate is of oscillating or non-oscillating character depends on the temperature, external electric field intensity E, and type of wide-band matrix, which carries studied QDs.

5. CONCLUSIONS

Our measurements reveal a rich spectrum of inelastic phonon-assisted electron tunneling processes in InAs/GaAs quantum dots. The number, position, and heights of the resonant peaks observed is well described with developed instanton approach extended to include effects of dissipative quantum tunneling. The good agreement with experiments has been achieved using a model in which an inelastic tunneling transition becomes allowed. There in the model of the wide-band matrix of InAs/GaAs quantum dots two phonon modes have been taken into account. The comparison between the experiments and developed theory allows us to probe electron-phonon interactions in this system and identify spectroscopically the energies and nature of the phonons emitted during the tunneling.

Practical implication of the obtained result is that the current-voltage characteristics of the semiconductor tunnel nanoelectronic devices can thus be controlled to a certain extent by modulations of the wide-band matrix parameters. For example, the quantum dots can serve as very sensitive detectors of properties of bulk materials used in precision nanoelectronics.

It is necessary to note that the theory for dissipative tunneling with the influence of two local phonon modes in the external electric field developed in this paper can be used in problems of resonant impurity states in quantum molecules in the case when the lifetime of the impurity electron is mainly determined by electron tunneling decay.

The problem of the influence of the electric field on the radiative recombination spectra of electrons and holes in a quantum dot is also of interest [29, 30]. In this case, the electron tunneling between a quantum dot and biological object can play an important role.

We are grateful to A.J. Leggett for his attention to this work; to B.N. Zvonkov (Research Institute for Physics and Technology, Lovachevsky State University of Nizhny Novgorod) for QD samples used in the CAFM experiment; to P.A. Borodin for assistance in the CAFM experiment, and to I.E. Bulyzhenkov and Yu.N. Ovchinnikov for useful discussions. A part of this work was done in the framework of the state contract with the Ministry of Education and Science of the Russian Federation. The work of A.K.A., M.B.S.,

and V.D.K. was supported in part by the Committee of Science, Ministry of Education and Science of Kazakhstan.

REFERENCES

1. A. O. Caldeira and A. J. Leggett, Phys. Rev. Lett. **46**, 211 (1981).
2. A. I. Larkin and Yu. N. Ovchinnikov, JETP Lett. **37**, 322 (1983).
3. I. E. Bulyzhenkov and B. I. Ivlev, Sov. Phys. JETP **47**, 115 (1978).
4. A. I. Larkin and Yu. N. Ovchinnikov, Sov. Phys. JETP **64**, 185 (1986).
5. Y. Imry, *Introduction to Mesoscopic Physics* (Oxford Univ. Press, Oxford, 2008).
6. *Transfer Processes in Low-Dimensional Systems,* Collection of Articles, Dedicated to the Prof. A.A. Ovchinnikov and Prof. A.I. Larkin's Memory, Ed. by Yu. I. Dahnovsky, V. D. Krevchik, V. Ya. Krivnov, M. B. Semenov, and K. Yamamoto (UT Res. Inst. Press, Tokyo, 2005).
7. *Controllable Dissipative Tunneling. Tunneling Transport in Low-Dimensional Systems,* Ed. by A. J. Leggett (Fizmatlit, Moscow, 2012).
8. A. Venkatesan, K. J. Lulla, V. J. Patton, A. D. Armour, C. J. Mellor, and J. R. Owers-Bradley, Phys. Rev. B **81**, 073410 (2010).
9. Yu. Bomze, H. Mebrahtu, I. Borzenets, A. Makarovski, and G. Finkelstein, Phys. Rev. B **79**, 241402(R) (2009).
10. D. K. Ferry, S. M. Goodnick, and J. Bird, *Transport in Nanostructures* (Cambridge Univ. Press, Cambridge, 2009).
11. L. G. G. V. Dias da Silva and E. Dagotto, Phys. Rev. B **79**, 155302 (2009).
12. A. Grodecka, P. Machnikowski, and J. Forstner, Phys. Rev. B **78**, 085302 (2008).
13. Yu. Dahnovsky, A. A. Ovchinnikov, and M. B. Semenov, Sov. Phys. JETP **65**, 541 (1987).
14. Yu. I. Dahnovsky and M. B. Semenov, J. Chem. Phys. **91**, 7606 (1989).
15. V. F. Gantmakher and M. V. Feigel'man, Phys. Usp. **41**, 105 (1998).
16. A. K. Aringazin, Yu. Dahnovsky, V. D. Krevchik, M. B. Semenov, A. A. Ovchinnikov, and K. Yamamoto, Phys. Rev. B **68**, 155426 (2003).
17. Yu. I. Dahnovsky, A. A. Ovchinnikov, and M. B. Semenov, Mol. Phys. **63**, 497 (1988).
18. V. Ch. Zhukovsky, O. N. Gorshkov, V. D. Krevchik, M. B. Semenov, E. V. Groznaya, D. O. Filatov, and D. A. Antonov, Moscow Univ. Phys. Bull. **64**, 27 (2009).
19. V. Ch. Zhukovsky, Yu. I. Dahnovsky, O. N. Gorshkov, et al. (Collab.), Moscow Univ. Phys. Bull. **64**, 475 (2009).
20. V. Ch. Zhukovsky, Yu. I. Dahnovsky, V. D. Krevchik, M. B. Semenov, V. G. Mayorov, E. I. Kudryashov, E. V. Shcherbakov, and K. Yamamoto, Moscow Univ. Phys. Bull. **62**, 73 (2007).
21. Supplementary material for this paper at http://link.springer.com/.
22. A. A. Bukharaev, N. V. Berdunov, D. V. Ovchinnikov, and K. M. Salikhov, Russ. Microelectron. **26**, 137 (1997).
23. K. M. Lang, D. A. Hite, R. W. Simmonds, R. Mc. Dermott, D. P. Pappas, and J. M. Martinis, Rev. Sci. Instrum. **75**, 2726 (2004).
24. K. Suzuki, K Kanisawa, C. Janer, S. Perraud, K. Takashina, T. Fujisawa, and Y. Hirayama, Phys. Rev. Lett. **98**, 136802 (2007).
25. P. A. Borodin, A. A. Bukharaev, D. O. Filatov, D. A. Vorontsov, and M. A. Lapshina, J. Surf. Invest.: X-ray, Synchrotr., Neutron Tech. **3**, 721 (2009).
26. D. Filatov, V. Shengurov, N. Nurgazizov, P. Borodin, and A. Bukharaev, in *Fingerprints in the Optical and Transport Properties of Quantum Dots,* Ed. by A. Al-Ahmadi (InTech, Croatia, 2012), p. 273.
27. O. Stier, M. Grundmann, and D. Bimberg, Phys. Rev. B **59**, 5688 (1999).
28. T. Maltezopoulos, A. Bolz, Ch. Meyer, Ch. Heyn, W. Hansen, M. Morgenstern, and R. Wiesendanger, Phys. Rev. Lett. **91**, 196804 (2003).
29. G. G. Zegrya, Tech. Phys. Lett. **32**, 174 (2006).
30. G. G. Zegrya and D. M. Samosvat, J. Exp. Theor. Phys. **108**, 907 (2009).